

Electronic Supplementary Information

Breaking aggregation in a tetrathiafulvalene-fused zinc porphyrin by metal-ligand coordination to form a donor-acceptor hybrid for ultrafast charge separation and charge stabilization

Atanu Jana,^a Habtom B. Gobeze,^b Masatoshi Ishida,^c Toshiyuki Mori,^d Katsuhiko Ariga,^{ae} Jonathan P. Hill^{*ae} and Francis D'Souza,^{*b}

^a*Supermolecules Group, WPI center for Materials Nanoarchitectonics, National Institute for Materials Science (NIMS), Namiki 1-1, Tsukuba, Ibaraki 3050044, Japan. E-mail: jonathan.hill@nims.go.jp*

^b*Department of Chemistry, University of North Texas, 1155 Union Circle, 305070, Denton, Texas 76203-5017, United States.*

E-mail: Francis.DSouza@UNT.edu

^c*Education Center for Global Leaders in Molecular Systems for Devices, Kyushu University, Fukuoka 819-0395, Japan.*

^d*Fuel Cell Materials Group, National Institute for Materials Science (NIMS), Namiki 1-1, Tsukuba, Ibaraki 3050044, Japan.*

^e*JST-CREST, Gobancho, Chiyoda-ku, Tokyo 102-0075, Japan*

Contents

1.0 Supplementary Figures

Fig. S1. Absorption spectral changes during increased addition of NOSbF₆

Fig. S2. Femtosecond transient absorption spectrum of (TTF)₄PZn

2.0 Characterization data for TTF-porphyrins

Fig. S3. HPLC-GPC traces

Fig. S4. ¹H NMR spectrum of (TTF)₄PH₂

Fig. S5. ¹³C NMR spectrum of (TTF)₄PH₂

Fig. S6. MALDI-TOF-MS spectrum of (TTF)₄PH₂

Fig. 7. ¹H NMR spectrum of (TTF)₄PZn

Fig. 8. ¹³C NMR spectrum of (TTF)₄PZn

Fig. 9. MALDI-TOF-MS spectrum of (TTF)₄PZn

Fig. S10. Optimized geometry of the (TTF)₄PZn and (TTF)₄PZn:C₆₀Im

Fig. S11. Molecular Orbital (MO) energy diagram for (TTF)₄PZn

Fig. S12. Molecular Orbital (MO) energy diagram for C₆₀Im

Fig. S13. Molecular Orbital (MO) energy diagram for dyad (TTF)₄PZn:C₆₀Im

1. Supplementary Figures

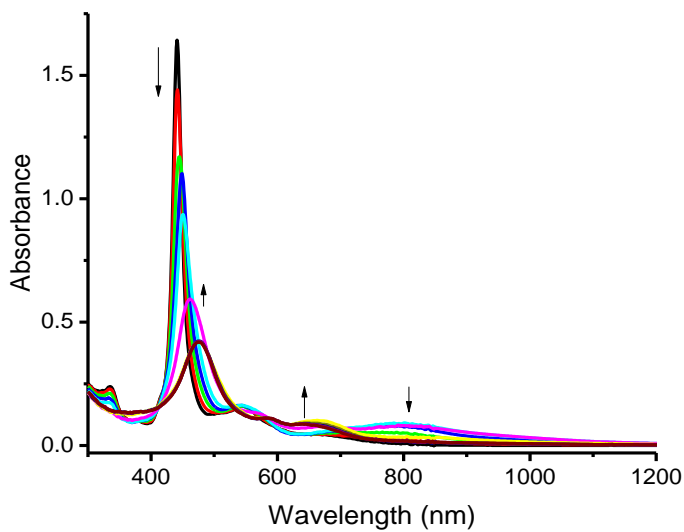


Fig. S1. Absorption spectral changes observed during increased addition of nitrosonium hexafluoroantimonate (0.2 equivalent each addition) to a solution of $(\text{TTF})_4\text{PZn}$ in DCB.

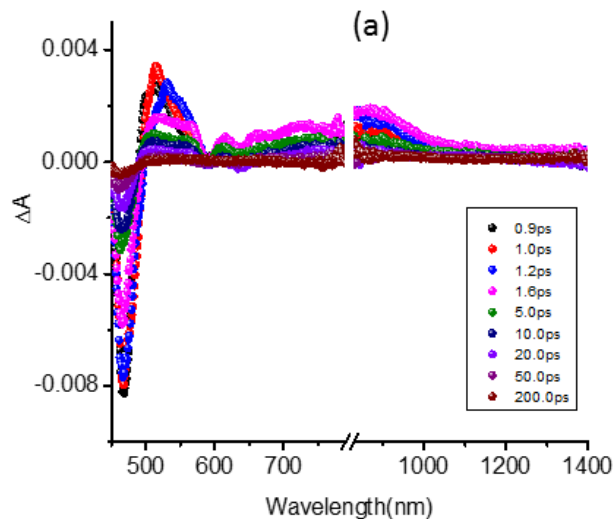


Fig. S2. Femtosecond transient absorption spectrum of $(\text{TTF})_4\text{PZn}$ at the indicated time intervals in DCB.

2.0 Characterization data for $(\text{TTF})_4\text{PH}_2$ and $(\text{TTF})_4\text{PZn}$

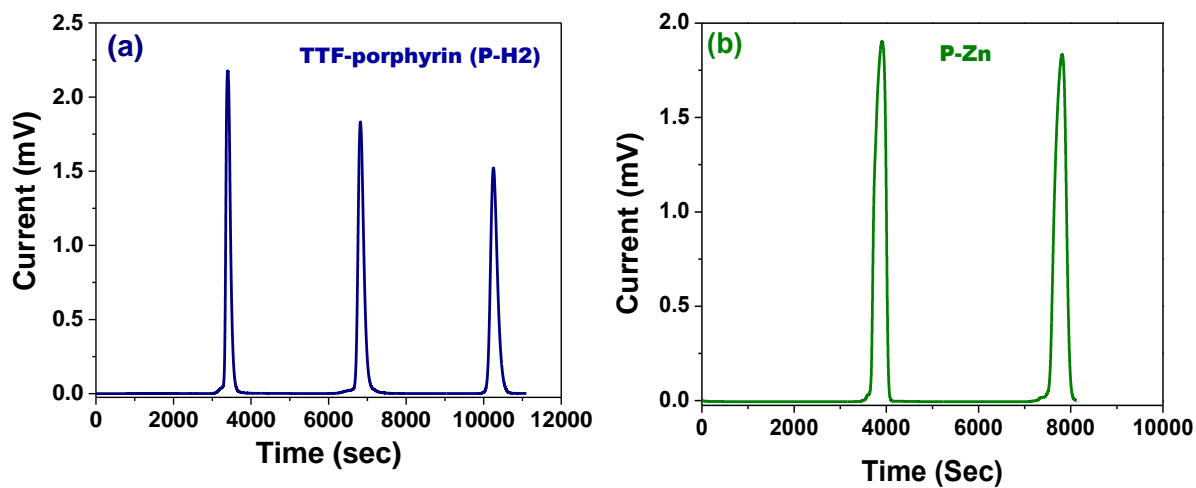


Fig. S3. Partial HPLC-GPC traces for the free base $(\text{TTF})_4\text{PH}_2$, (a); and its corresponding Zn(II)-complex, $(\text{TTF})_4\text{PZn}$, (b) used in this study.

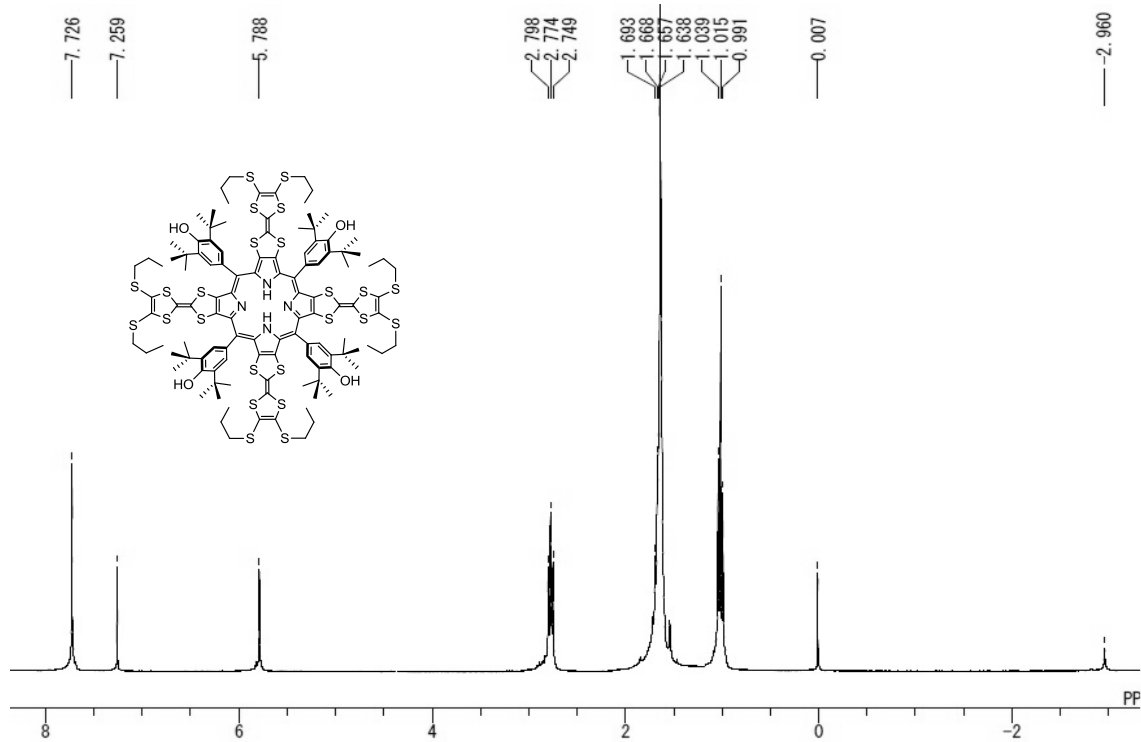


Fig. S4. ^1H NMR spectrum (300 MHz) of $(\text{TTF})_4\text{PH}_2$ recorded in CDCl_3 at 298 K.

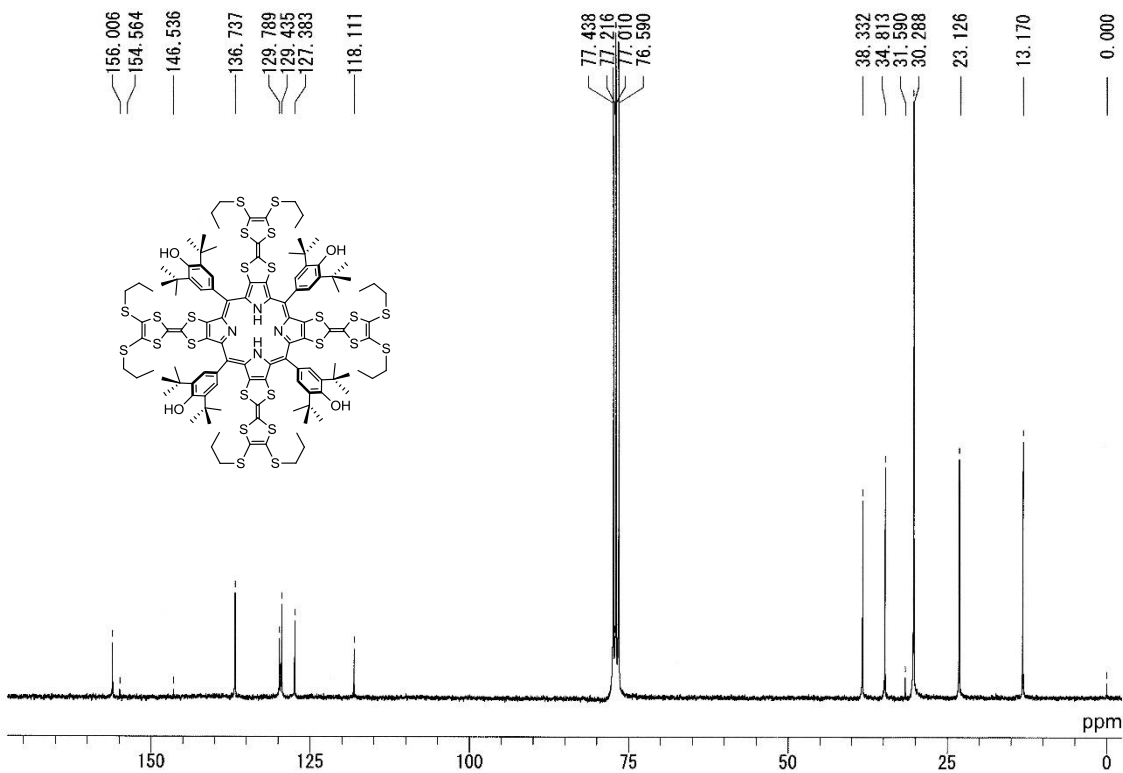


Fig. S5. ^{13}C NMR spectrum (75 MHz) of $(\text{TTF})_4\text{PH}_2$ recorded in CDCl_3 at 298K.

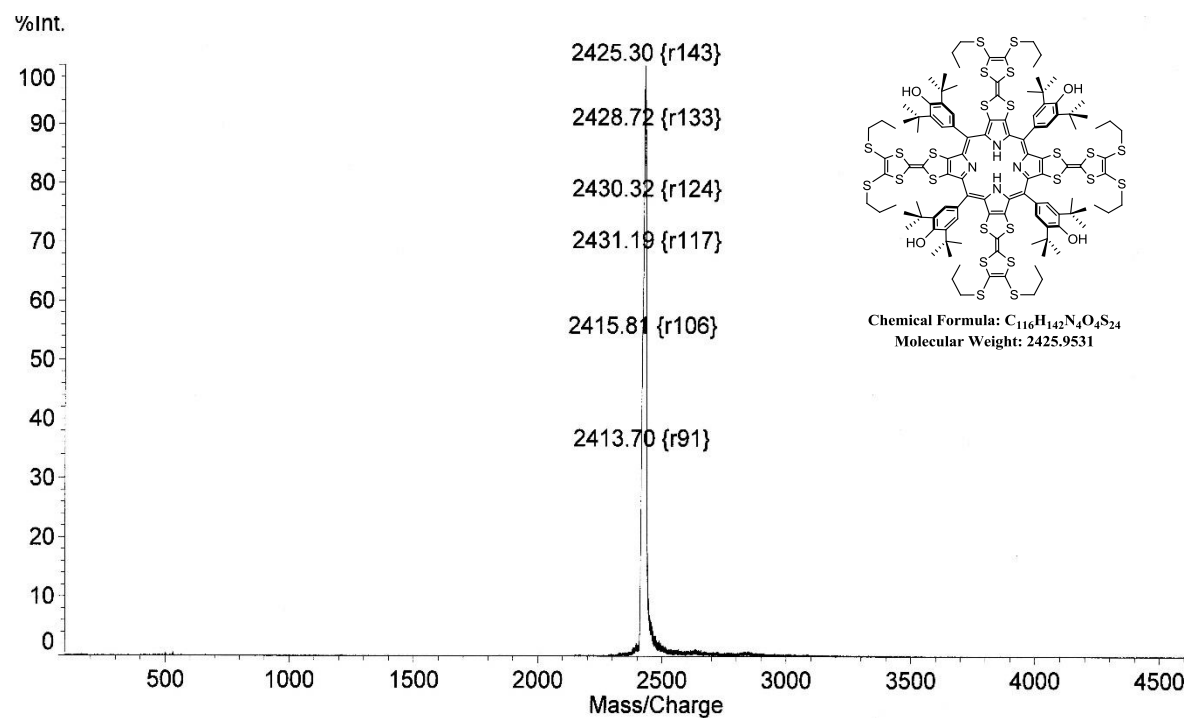


Fig. S6. MALDI-TOF mass spectrum of (TTF)₄PH₂.

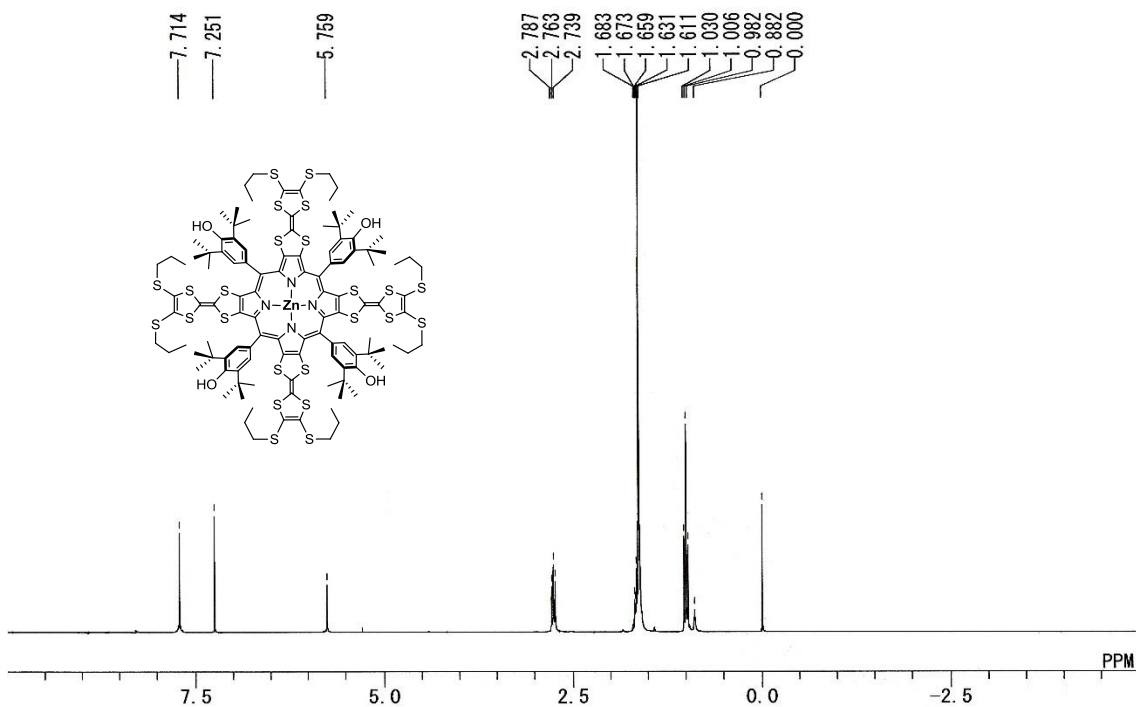


Fig. S7. ^1H NMR spectrum (300 MHz) of $(\text{TTF})_4\text{PZn}$ recorded in CDCl_3 at 298 K.

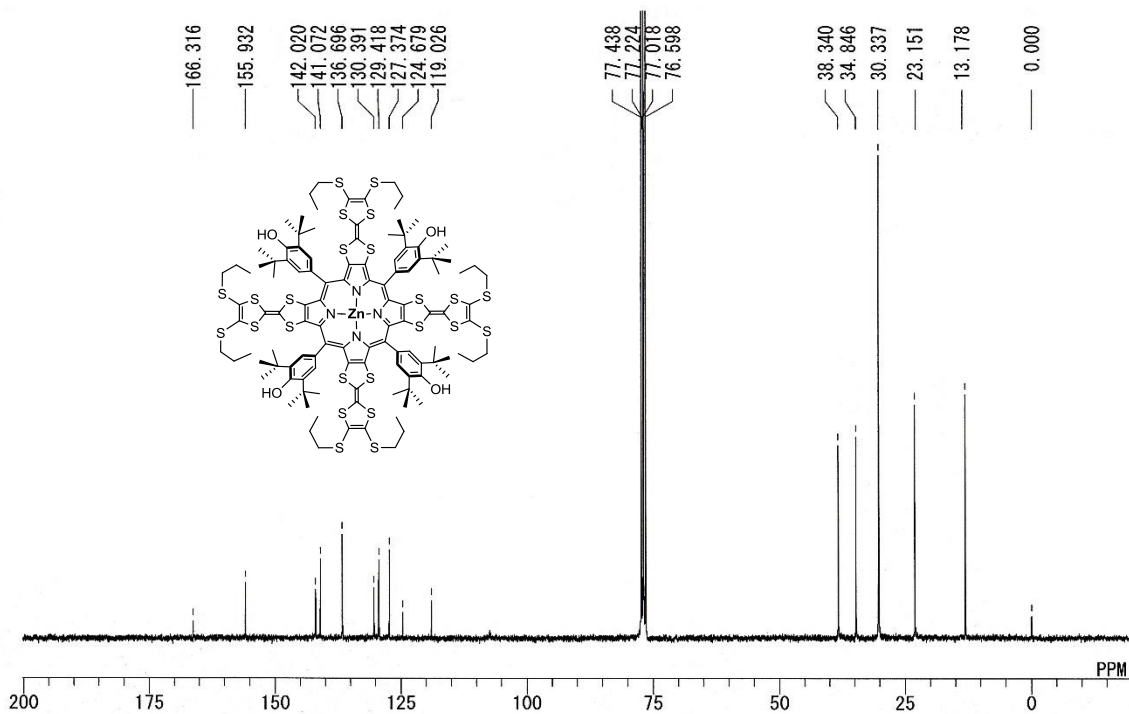


Fig. S8. ^{13}C NMR spectrum (75 MHz) of $(\text{TTF})_4\text{PZn}$ recorded in CDCl_3 at 298 K.

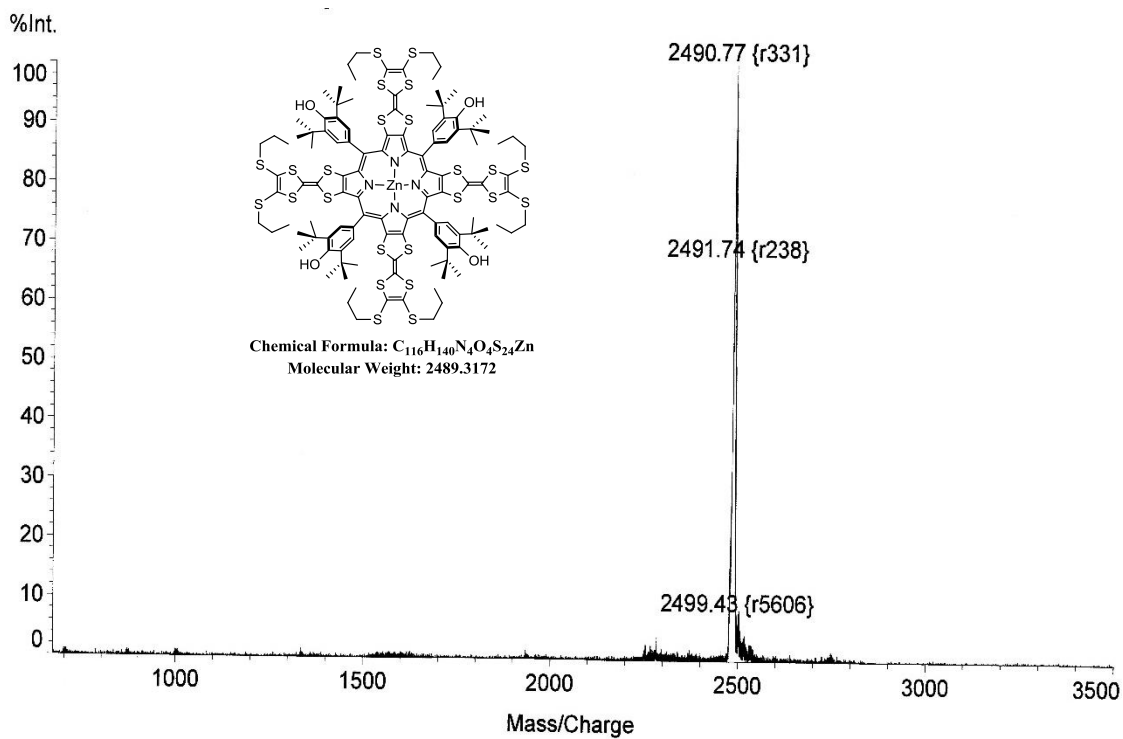


Fig. S9. MALDI-TOF mass spectrum of $(TTF)_4PZn$.

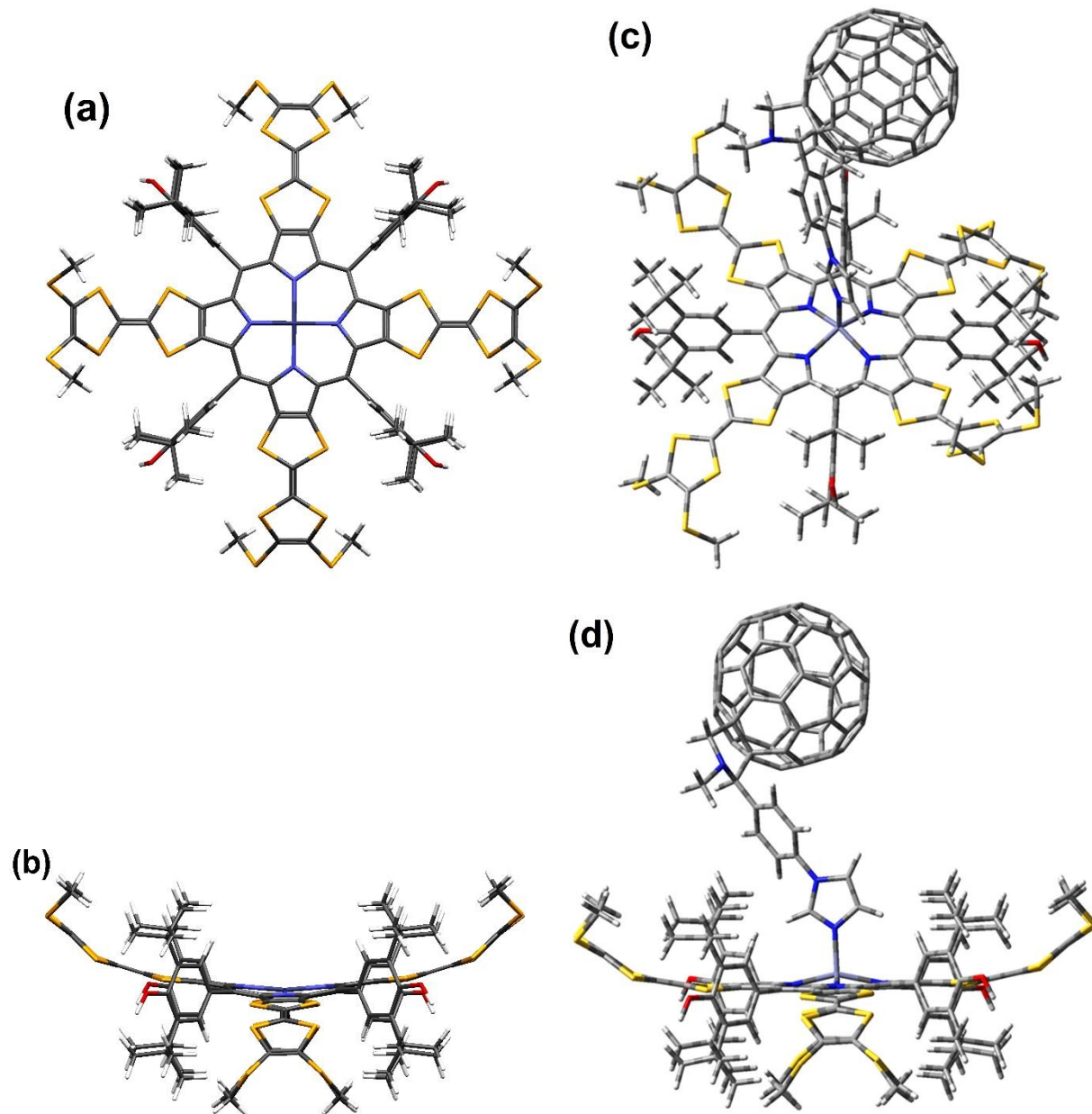


Fig. S10. Optimized geometry of the $(\text{TTF})_4\text{PZn}$, (a) top view, (b) side view along with its supramolecular dyad $(\text{TTF})_4\text{PZn}:\text{C}_60\text{Im}$; (c) top view, (d) side view, respectively.

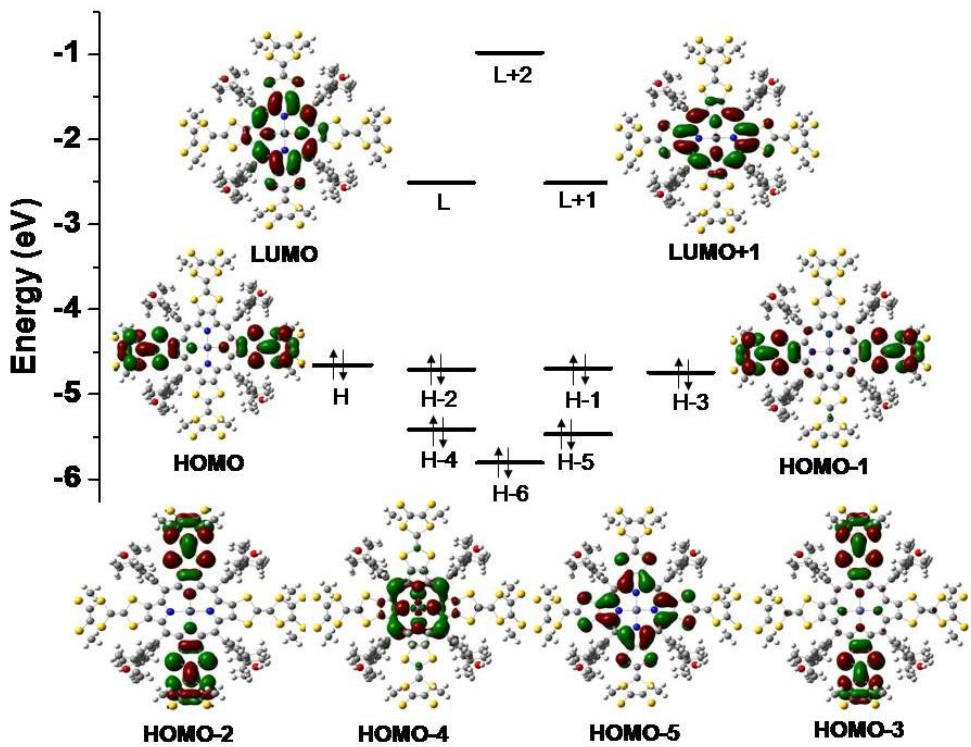


Fig. S11. Molecular Orbital (MO) energy diagram for (TTF)₄PZn.

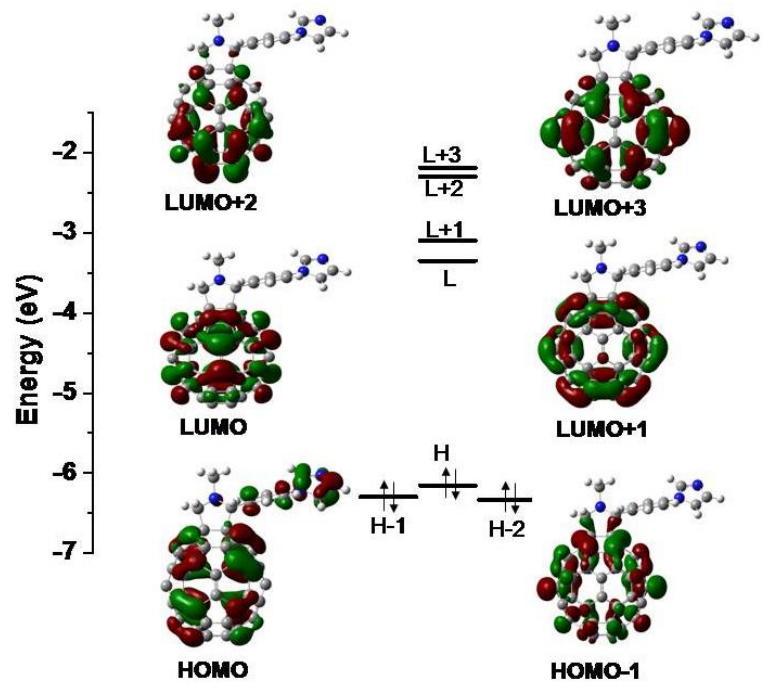


Fig. S12. Molecular Orbital (MO) energy diagram for $C_{60}Im$.

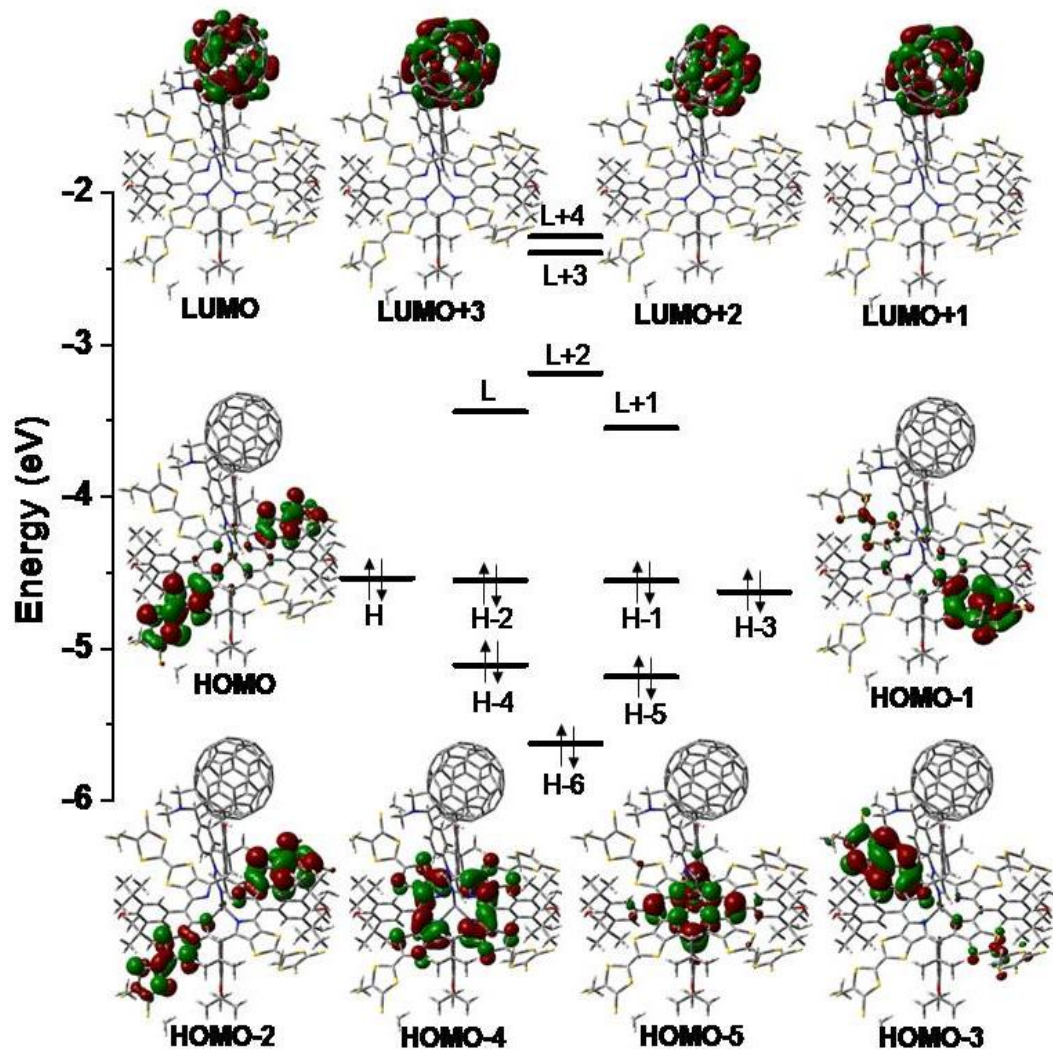


Fig. S13. Molecular Orbital (MO) energy diagram for the supramolecular dyad (TTF)₄PZn:C₆₀Im used in this study.